REPORT DOCUMENTATION PAGE

Form Approved
OMB No. 0704-0188

1. REPORT DATE *(DD-MM-YYYY)*	**2. REPORT TYPE**	**3. DATES COVERED** *(From - To)*
21-12-2011	Final Report	30-Sep-2010 TO 29-Sep-2011

4. TITLE AND SUBTITLE

SUPPLEMENTAL TASK - HIGH POWER LASERS

5a. CONTRACT NUMBER

5b. GRANT NUMBER

FA9550-10-1-0562

5c. PROGRAM ELEMENT NUMBER

6. AUTHOR(S)

Prof. Luke Lester, Prof. Ganesh Balakrisnan

5d. PROJECT NUMBER

5e. TASK NUMBER

5f. WORK UNIT NUMBER

7. PERFORMING ORGANIZATION NAME(S) AND ADDRESS(ES)

UNM Center for high technology materials, MSC 04-2710,
1313 Goddard SE, Albuquerque, NM 87106.

8. PERFORMING ORGANIZATION REPORT NUMBER

9. SPONSORING / MONITORING AGENCY NAME(S) AND ADDRESS(ES)

Air Force Office of Scientific Research
875 North Randolph St.
Arlington, VA 22203

10. SPONSOR/MONITOR'S ACRONYM(S)

11. SPONSOR/MONITOR'S REPORT NUMBER(S)

AFRL-OSR-VA-TR-2012-0807

12. DISTRIBUTION / AVAILABILITY STATEMENT

Unlimited

13. SUPPLEMENTARY NOTES

14. ABSTRACT

The researchers made significant progress in all of the proposed research areas. The first task involved the growth and characterization of 1040 nm vertical external cavity surface emitting lasers (VECSELs). These devices have been grown by MOCVD and have been subjected to temperature-dependent reflectivity studies to optimize the alignment of the gain peak with the micro-cavity as well as examining their continuous wave output power properties. Secondly, based on extensive electronic structure simulations, single and dual tunnel-injection based quantum dot epi-structures have been designed. These structures leverage from the already established world-class quantum dot VECSEL research at CHTM.

15. SUBJECT TERMS

Vertical external cavity surface emitting lasers, crystal growth, semiconductor laser epi-structure design, quantum wells, quantum dots.

16. SECURITY CLASSIFICATION OF:			**17. LIMITATION OF ABSTRACT**	**18. NUMBER OF PAGES**	**19a. NAME OF RESPONSIBLE PERSON**
a. REPORT	**b. ABSTRACT**	**c. THIS PAGE**		14	Prof. Luke F. Lester
					19b. TELEPHONE NUMBER *(include area code)* 505-272-7801

Final Performance Report

Grant FA9550-10-1-0562

09/30/2010-09/29/2011

Prof. Luke F. Lester, Prof. Ganesh Balakrishnan

December 20, 2011

Abstract

The researchers made significant progress in all of the proposed research areas. The first task involved the growth and characterization of 1040 nm vertical external cavity surface emitting lasers (VECSELs). These devices have been grown by MOCVD and have been subjected to temperature-dependent reflectivity studies to optimize the alignment of the gain peak with the micro-cavity as well as examining their continuous wave output power properties. Secondly, based on extensive electronic structure simulations, single and dual tunnel-injection based quantum dot epi-structures have been designed. These structures leverage from the already established world-class quantum dot VECSEL research at CHTM.

Overview: The effort from the University of New Mexico in the past year has been focused on developing epitaxial structures that have the ability to be operated CW under high pump power conditions with a target emission wavelength of 1040 nm as well as wavelengths associated with InAs quantum dots of 1240 nm [1,2]. The laser structures have been grown as top emitter structures with the active region on the top and the distributed Bragg reflector (DBR) on the bottom. The development of the VECSELs was delayed during this year due to the installation process for the AFOSR DURIP funded GEN 10 MBE reactor. Despite unforeseen delays on our MBE machine, we have made use of our MOCVD growth capabilities to ensure production of the first round of VECSEL devices. The current status of the experiment is that we are at the stage where chips are being packaged with diamond heat spreaders to enable high power performance [1-3]. With the completion of this step we shall proceed to send the chips out for various levels of anti-reflection coating. In parallel, our team has embarked on ameliorating our quantum dot VECSELs technologies [1-3]. Accordingly, novel single and dual coupled quantum dot-quantum well gain materials have been designed using an 8-band **k.p** approach. Knowledge of the temperature performance of this material system is of profound importance to ensure the optimization of our VECSELs. Previously, we have used the segmented contact method to acquire a better understanding of the temperature dependence of the gain and loss spectra in dots-in-a-well active regions [4,5]. These previous studies act as a valuable baseline for future work by giving us valuable insight into the temperature dependencies seen in semiconductor laser active regions.

Research team: The following personnel have been engaged in this work: Prof. Luke Lester, Prof. Ganesh Balakrishnan, Dr. Alex Albrecht, Dr. Mark Crowley and PhD candidates Nishant

Patel and Andy Liu. Nishant Patel has now completed his academic requirements and is currently preparing his PhD proposal for Spring 2012.

Epitaxy: The most critical aspect of this work done to date on this project is the ability to align the three components of the VECSEL micro-cavity structure. The process developed to achieve such precise growth involves three steps –

(a) coarse adjustments – This method involves a very careful calibration of the growth parameters in the machine using reflective high energy electron diffraction which provides us the growth rates required to within a percentage of the targeted growth rate. The first run in a series is then a VECSEL sample where the micro-cavity is grown simply based on such a process of calibrations. The typical result from such a calibration process is the misalignment of the microcavity structure with respect to the gain peak. The gain peak in all of the structures is kept at 1020 nm and the targeted micro-cavity dip is at 1040 nm. The quantum wells are based on InGaAs with GaAs spacer layers with the entire structure designed as a resonant periodic gain structure. This results in the QWs being placed at the antinodes of the standing wave electric-field created in a VECSEL.

(b) Precise alignment – In this step the reactor is kept very stable from the previous coarse calibration run and depending upon the extent of the microcavity is misaligned from the designed wavelength, an adjustment is made to the growth structure. If the misalignment is too large the barriers are adjusted. To our knowledge this is the only research effort that has developed such a technique for precise correction of the micro cavity alignment.

Characterization: Upon completion of the epitaxial process the samples are analyzed using a temperature dependent reflectivity setup which has been setup at UNM. If a further adjustment is

required in the growth then the structure is repeated again. The samples have all been tested for CW lasing as well as uniformity of lasing across the wafer. The samples are then lapped, polished, and metalized. The samples are subsequently mounted on a diamond substrate. The selected VECSEL chips will be tested and sent out for anti-reflection coating.

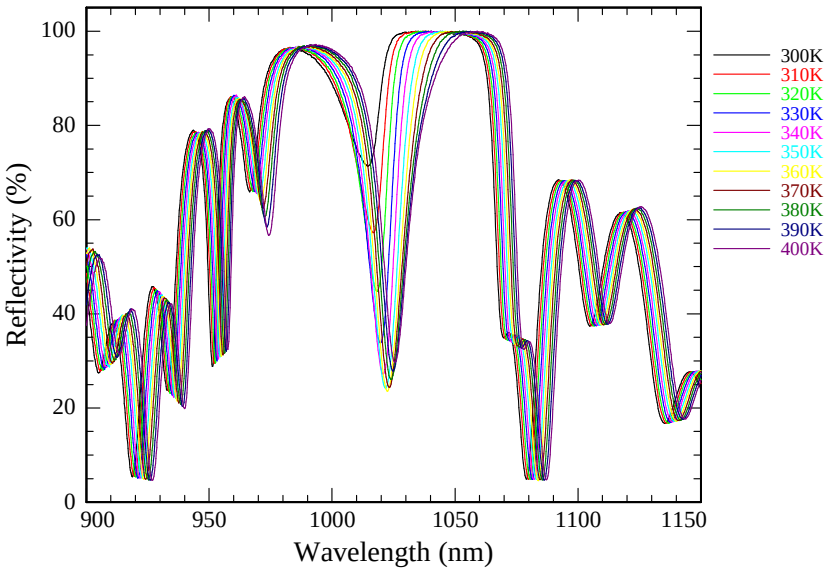

Fig. 1: Temperature dependent reflectivity showing the temperature at which the gain peak and the micro-cavity resonance are aligned at the target wavelength of 1040 nm.

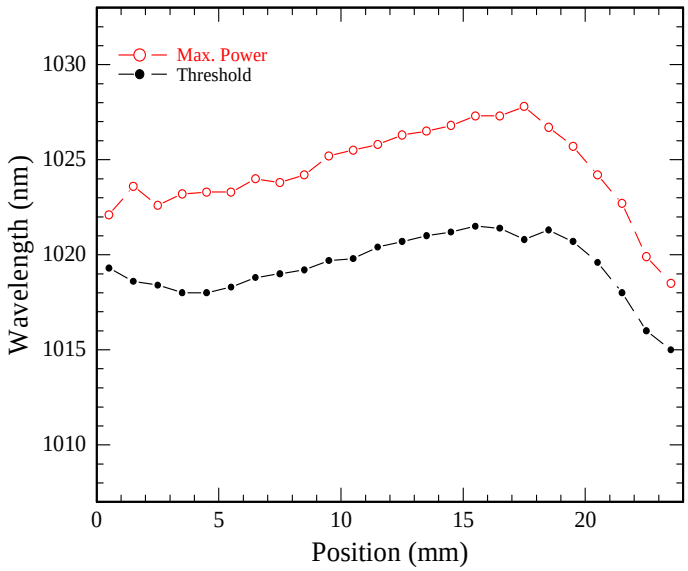

Fig. 2: Temperature dependent reflectivity showing the temperature at which the gain peak and the micro-cavity resonance are aligned.

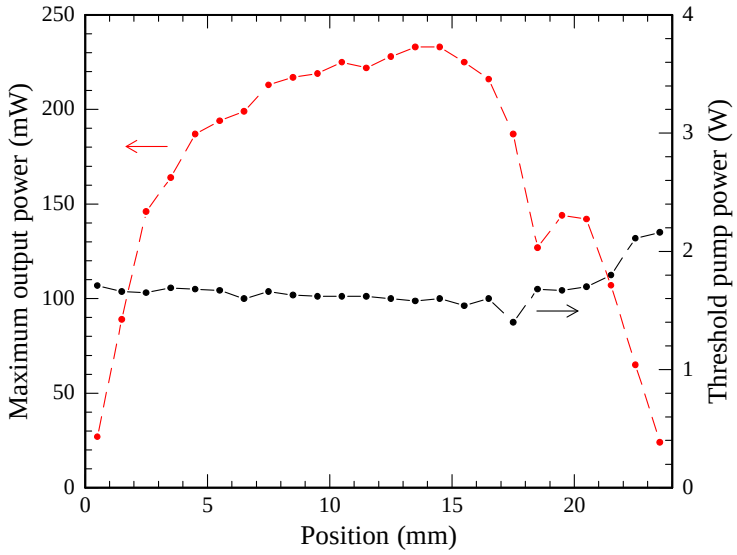

Fig. 3: Variation of maximum output power and threshold pump powers as a function of position relative to the center of the VECSEL wafer.

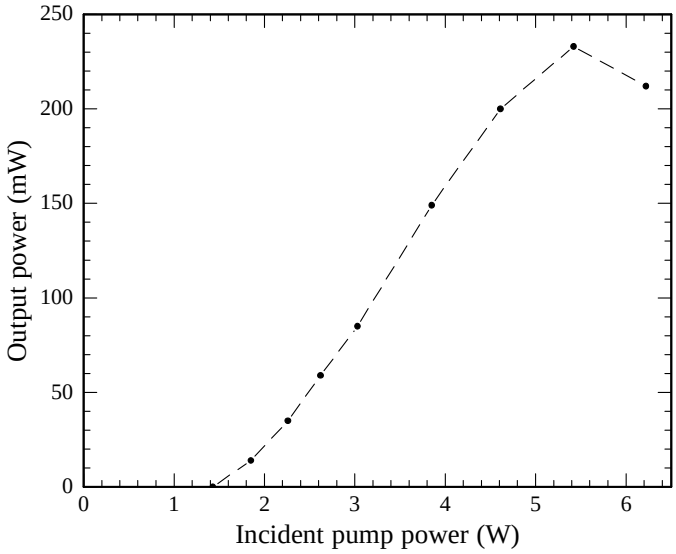

Fig. 4: L-L curve for the VECSEL under continuous wave conditions.

Coupled quantum dot-quantum well gain material designs:

Although the quantum dot active region is known to exhibit excellent temperature performance, it still suffers from hot carrier effects [6]. Among the underlying causes are an inhibited carrier energy relaxation in the dots stemming from the discrete nature of the allowed energy levels. By electronically coupling the lasing states of the dots with the minimum electron energies of a quantum well, cold carriers can be injected via phonon-assisted tunneling into the dots, thereby bypassing the natural inefficient relaxation route which generally results in a heating of the carrier distribution. Here we report on both single and dual carrier injection epi-structure designs to be incorporated into the VECSEL active region as an approach to mitigating hot carrier effects.

For these designs the ability to realistically describe the electron and hole energy distributions in the dots is essential to allow for an accurate lineup of the dot lasing states with the injector well

energy minimum. The calculations leading to the following designs have been performed using an 8 band **k·p** approach using a Fourier transform technique [7]. The report appendix contains details of the calculations used for designing the structures. Material parameters used in the calcualtions were adapted from Vurgaftman et al. [8] and are cross-correlated with published experimental characterizations of both InGaAs based dots and wells. The mean ensemble dot structure is assumed to have a square-based truncated pyramidal shape being 15 nm at the base and 6 nm in height. Figures 5-8 show our 4 designs. The designs are leveraged from our 12 stack QD VECSEL structures [1]. Figure 5 depicts a single tunnel injector design where the InGaAs injector well is chosen to inject cold electrons into the dense region of electron states just inside the dot energy potential. Figure 6 is also a single tunnel injector where the target state is the first excited state (ES) of the QDs. Tunnel injection into the dot ES requires a wider injector well and an increased amount of indium than the design shown in figure 5 since it is lower in energy than the latter. Figures 7 and 8 present dual carrier injection designs. The first design is a symmetric design which selectively populates the QD ES, simultaneously injecting cold electrons and holes into the QD ES. The second design is an asymmetric design which aims to target the dense set of carrier states for electrons and QD ES for holes. The inclusion of thin GaP layers are incorporated to offset the accumulation of compressive strain relative to growth on GaAs substrates. Following the periodic gain structure concept, each design constrains the thickness of the GaAs spacer layers such that the gain peak from the quantum dot ground state (GS) transition coincides with the minima of the standing electric field of the micro-cavity.

Layer name	Layer thickness	Notes
GaAs	168 nm	
$In_{0.15}Ga_{0.85}As$	6 nm	
InAs	2.5 ML	
$In_{0.15}Ga_{0.85}As$	1 nm	
GaAs/GaP	2 nm	Tunnel barrier: 0.5nm GaAs+1nm GaP+0.5nm GaAs
$In_{0.20}Ga_{0.85}As$	5 nm	Electron injector to highly excited dot levels

Fig. 5: 12 stack, 20% indium InGaAs single tunnel injector DWELL VECSEL active region

Layer name	Layer thickness	Notes
GaAs	163 nm	
$In_{0.15}Ga_{0.85}As$	6 nm	
InAs	2.5 ML	
$In_{0.15}Ga_{0.85}As$	1 nm	
GaAs/GaP	3 nm	Tunnel barrier: 0.5nm GaAs+2.5nm GaP+0.5nm GaAs
$In_{0.28}Ga_{0.72}As$	9 nm	Electron injector to dot ES

Fig. 6: 12 stack, 28% indium InGaAs single tunnel injector DWELL VECSEL active region

Layer name	Layer thickness	Notes
GaAs	156 nm	
$In_{0.28}Ga_{0.72}As$	9 nm	Hole injector to dot ES
GaAs	3 nm	Tunnel barrier: 0.5nm GaAs+2.5nm GaP+0.5nm GaAs
$In_{0.15}Ga_{0.85}As$	6 nm	
InAs	2.5 ML	
$In_{0.15}Ga_{0.85}As$	1 nm	
GaAs	2 nm	Tunnel barrier: 0.5nm GaAs+1nm GaP+0.5nm GaAs
$In_{0.20}Ga_{0.80}As$	5 nm	Electron injector to highly excited dot levels

Fig. 7: 12 stack, 28% indium dual InGaAs tunnel injector DWELL VECSEL active region.

Layer name	Layer thickness	Notes
GaAs	151 nm	
$In_{0.28}Ga_{0.72}As$	9 nm	Hole injector to dot ES
GaAs	3 nm	Tunnel barrier: 0.5nm GaAs+2.5 nm GaP+0.5nm GaAs
$In_{0.15}Ga_{0.85}As$	6 nm	
InAs	2.5 ML	
$In_{0.15}Ga_{0.85}As$	1 nm	
GaAs	3 nm	Tunnel barrier: 0.5nm GaAs+2.5 nm GaP+0.5nm GaAs
$In_{0.28}Ga_{0.72}As$	9 nm	Electron injector to dot ES

Fig. 8: 12 stack dual InGaAs tunnel injector DWELL VECSEL active region. 28% indium InGaAs tunnel injector for holes and a 20% indium InGaAs tunnel injector for electrons.

Appendix:

The appropriate thickness of the GaP strain-compensating layer is computed using continuum elasticity theory using equation (1) [9].

$$t_b = t_{sl}\left[\frac{A_{sl}\, a_b^2 \left(a_0 - a_{sl}\right)}{A_b\, a_{sl}^2 \left(a_b - a_0\right)}\right] \tag{1}$$

The subscripts denote strained layer, balancing layer, and substrate, as *sl*, *b*, and 0, respectively. Equation 1 includes both the material lattice constants, a_i, and their stiffness coefficients which are contained within the constant A_i of the alternating materials. This constant A is described in (2) where C represents stiffness coefficients of the ith layer material.

$$A_i = C_{11,i} + C_{12,i} - \frac{2C_{12,i}^2}{C_{11,i}} \tag{2}$$

Since the impact of strain on the confinement energies is comparable to that of the band offsets at the heterojunctions, the wavefunctions and energies are very sensitive to the underlying strain distribution in the structure. The impact of the model used for calculating the strain distribution has been analyzed in a number of publications where the continuum elastic model was shown to be the optimal choice for the current implementation of the 8-band **k.p** model. The total strain energy of the continuum mechanical (CM) model is given by [10]

$$U_{CM} = \frac{1}{2}\sum_{i,j,k,l} C_{ijkl}\varepsilon_{ij}\varepsilon_{kl} \tag{3}$$

The strain values are defined as $\varepsilon_{ij}=\partial u_i/\partial x_j$, where u is the displacement vector field. The strain values need to be determined in order to minimize U for a given structure. The compliances, C_{ijkl}, are represented by the parameters C_{11}, C_{12}, and C_{44} for cubic crystals.

To compute a realistic distribution of electron and hole levels within the dots and wells of the epi-structures, we use an 8-band **k.p** model which in addition to the strain energy also includes energy band-mixing and spin-orbit coupling. The 8-band **k.p** Hamiltonian takes the following generalized form [10, 11]

$$\hat{H} = \begin{pmatrix} G[k] & \Gamma \\ -\overline{\Gamma} & \overline{G}[k] \end{pmatrix} \tag{4}$$

where $G[\mathbf{k}]$ and Γ are 4×4 matrices and the overlining denotes the complex conjugate of the matrix. The matrix Γ describes the spin-orbit splitting while G is composed of a potential energy part G_1, a kinetic energy part G_2, a spin-orbit interaction part G_{SO}, and a strain dependent part G_{st} :

$$G = G_1 + G_2 + G_{SO} + G_{st} \tag{5}$$

For each material layer in the epi-structure, the 8-band **k.p** Hamiltonian considers the following inputs:

1). the fundamental band gap E_0,

2). the spin-orbit energy Δ_{s0},

3). the optical matrix parameter E_p,

4). the valence band edge E_v ,

5). the relative Γ -point conduction band mass m_e,

6). the three Luttinger parameters γ_1, γ_2 , and γ_3,

7). the Kane parameter B,

8). the hydrostatic conduction band deformation potential a_c,

9). the hydrostatic band gap deformation potential a_g,

10). the uniaxial ([100] direction) valence band deformation potential b_v,

11). the uniaxial ([111] direction) valence band deformation potential d_v,

12). the parameter b' coupling the conduction band edge to shear strain,

13). and an optional scalar potential V_{ext} describing an electric field resulting from, for example, a built-in voltage in a p-n-junction, an externally applied voltage, or a piezoelectric charging.

To implement the 8-band electronic structure in this work we adopt a computationally efficient Fourier-space method that is particularly suited for studying electronic and optical properties of QDs and QDashes [7]. The method proceeds by computing the three-dimensional strain in and around the nanostructures. These are calculated from analytic expressions which include the Fourier transform of the characteristic function for the nanostructure shape. This input is then combined with a plane-wave expansion method for calculating the energies and wavefunctions in the QD and QDash structures [7]. Iterative calculations are performed to determine the optimum injector well indium composition and thickness required to hit resonance, within one LO phonon, of the target dot states.

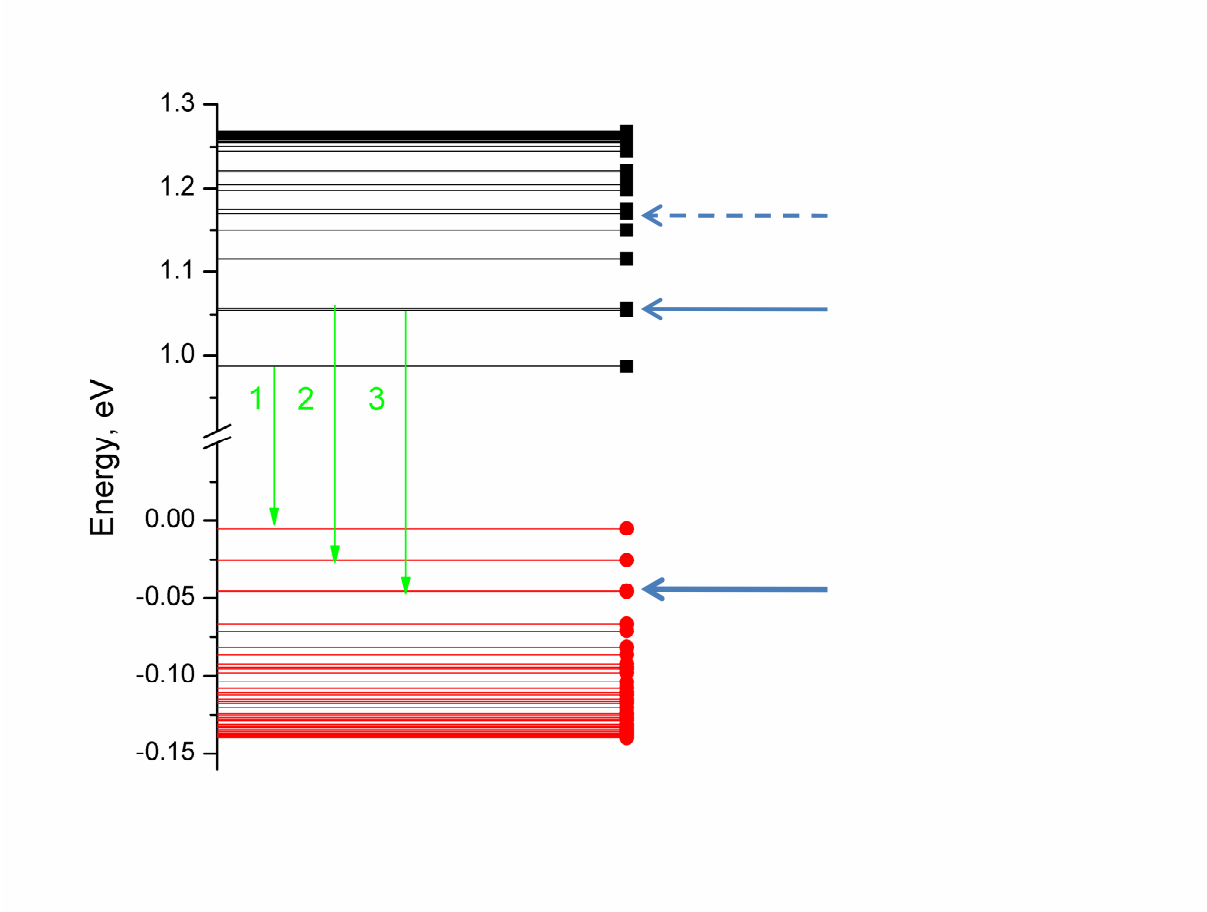

Fig. A1: Calculated electron (black squares) and hole (red circles) energies of an example quantum dot (15 nm base length). The cut-off energy for carriers denotes the onset of fully delocalized states. Green arrows depict the first three dominant transitions. Transition 1 involves both ground state electrons and holes. Transitions 2 and 3 are related to the first excited state peak and are observed qualitatively by quantum dot photoluminescence.. The horizontal arrows denote the targeted dot states for the injector wells.

References:

[1] Albrecht A R, Rotter, T J, Hains, C P, Stintz A, Moloney J V Malloy K J and Balakrishnan G Multi-watt 1.25 μm quantum dot VECSEL *Electron. Lett.* **46** 856-857, 2010.

[2] Albrecht A R, Hains C P, Rotter T J, Stintz A, Malloy K J, Balakrishnan G and Moloney J V High power 1.25 μm InAs quantum dot vertical external-cavity surface-emitting laser *J. Vac. Sci. Tech. B: Microelectronics and Nanometer Structures*, **29** 03C113 - 03C113-4, 2011.

[3] Albrecht A R, Stintz A, Jaeckel F T, Rotter T J, Ahirwar P, Patel V J, Hains C P, Lester L F, Malloy K J and Balakrishnan G 1220–1280-nm Optically Pumped InAs Quantum Dot-Based Vertical External-Cavity Surface-Emitting Laser, *IEEE J. Sel. Top Quantum Electron*. **17** 1787-1793, 2011.

[4] Crowley M T, Murrell D, Patel N, Breivik M, Lin C-Y, Li Y, Fimland B-O and Lester L F Analytical Modeling of the Temperature Performance of Monolithic Passively Mode-Locked Quantum Dot Lasers *J. Quantum Electron.* **47** 1059-1068, 2011.

[5] Xin, Y. C., Li, Y., Martinez, A., Rotter, T. J., Su, H., Zhang, L., Gray, A. L., Luong, S., Sun, K., Zou, Z., Zilko, J., Varangis, P. M., and Lester, L. F., Optical gain and absorption of quantum dots measured using an alternative segmented contact method, *IEEE J. Quantum Electron.* **42**, 725-732 2006.

[6] Crowley M T, Naderi N A, Su H, Grillot F and Lester L F GaAs-based Quantum Dot Lasers in *Semiconductors and Semimetals* vol on Advances in Semiconductor Lasers (New York: Academic), to be published June 2012.

[7] Andreev A D, O'Reilly E P, Theory of the electronic structure of GaN/AlN hexagonal quantum dots, *Phys. Rev. B*, **62**, 15851, 2000.\

[8] Vurgaftman I, Meyer J R and Ram-Mohan L R, Band parameters for III–V compound semiconductors and their alloys *J. Appl.Phys*. **89**, 5815, 2001.

[9] Bailey C G, Hubbard S M, Forbes D V and Raffaelle R P Evaluation of strain balancing layer thickness for InAs/GaAs quantum dot arrays using high resolution x-ray diffraction and photoluminescence *Appl. Phys. Lett*. **95** 203110, 2009.

[10] Stier O, Electronic and optical properties of quantum dots and wires, PhD thesis, Technical University of Berlin, (2000).

[11] Bahder T B, Eight-band **k·p** model of strained zinc-blende crystals, *Phys. Rev. B*, **41**, 11992 (1990).